Three-Component Sequential Reactions for Polymeric Nanoparticles with Tailorable Core and Surface Functionalities

Bin Liu[1] and S. Thayumanavan[1,2,3*]

[1]Department of Chemistry, [2]Center for Bioactive Delivery, Institute for Applied Life Sciences, [3]Molecular and Cellular Biology Program, University of Massachusetts, Amherst, Massachusetts 01003, USA.

*e-mail address: thai@chem.umass.edu.

ABSTRACT

Efficient strategies for the preparation of nanostructures with tailorable functionalities have implications in enhancing the repertoire of nanomaterials in many applications. Multi-component reactions (MCRs) are very attractive, because of their synthetic simplicity while providing unique access to incorporation of functional groups onto a system. This highly efficient process has not been brought to bear in the preparation of functional polymeric nanostructures. In this paper, we report a novel three-component sequential reaction that is capable of concurrently functionalizing the core or the surface of the nanoparticles and crosslinking the polymeric assemblies. Variations in core offer the opportunity to optimize the host-guest properties, while the surface features provide the ability to tune interfacial interactions. We demonstrate a tight control over the size of these nanoassemblies, from ~10 nm to ~1 μm. In addition, we also show that the surface functionalities of these assemblies can be conveniently varied, the utility of which has been further demonstrated in organelle targeting in cells. Similarly, functionalities in the core of these assemblies have also been tuned, which has been shown to have implications in the robust non-covalent encapsulation of guest molecules. The utility of this feature in efficiently encapsulating anti-cancer drug molecules and their delivery have been demonstrated. This one-pot, three-component sequential reaction affords the opportunity to prepare NPs with these unique properties through a simple and green chemical process.

NTRODUCTION

Nanoscale assemblies with sophisticated properties have attracted tremendous interest, because of the potential applications in different fields such as drug delivery, biomedical diagnostics, and theranostics.[1-5] Scaffolds such as inorganic nanoparticles[6,7], liposomes[8], dendrimers[9], polymeric assemblies[10-15], and polymer-based nanoparticles[10-16] have been explored for this purpose. Among these, amphiphilic block copolymer based assemblies have been extensively studied due to their water solubility and noncovalent encapsulation capabilities of hydrophobic guest molecules in aqueous phase.[10-16] These features are particularly important for therapeutic applications, where the ability to load hydrophobic drug molecules into a water-dispersible nanoassembly is critical for overcoming some of the pharmacokinetic limitations of conventional drug formulations.[17-20] Block polymeric micelles contain well-defined core-shell structure with hydrophobic polymer cores and water-soluble polymer shells. In order to achieve efficient drug encapsulation inside the core of the block polymer micelles, it requires the guest molecules to overcome the barrier formed by the shell layer and the oft-glassy core polymer block. There are usually two methods for drug encapsulation, which is based on the dissolution of the drug molecules and the block copolymers in a water-miscible organic solvent together with subsequent addition of water and further removal of the organic solvent by evaporation or dialysis to efficiently decrease the energy barrier for the drug molecules to penetrate from the micelle shell to the glassy hydrophobic core.[21-24] However, these methods are not suitable for scalable production as physical factors (e.g. diffusion and solvent exchange rate) are influenced heavily by the scales during the drug incorporation processes. Furthermore, there is also an environmental cost associated with using organic co-solvents in a process that is primarily driven by the propensity of the host assembly to self-assemble in water.[21-24]

Also, most disease models have disparate requirements in features such as size and surface functionalities to optimize their circulation time, as well as tissue, cellular and sub-cellular targeting.[25-27]

Note however that it is difficult to tune the size of micelles from one polymeric precursor in the case of block copolymers, as the assembly size here is controlled by the relative block composition and the block length under equilibrium conditions;[23, 24, 28, 29] *i.e.*, a polymer with the specific structure usually affords a micelle with a well-defined size.[23, 24, 28, 29] Therefore, when block copolymer micellar assemblies with different sizes are desired, a series of different polymers need to be designed and synthesized, which is time consuming and laborious.[30] In fact, it is difficult to prepare block copolymer based micelles with small ($d<20$ nm) and big ($d>100$ nm) sizes.[28-32] Moreover, the surface functional groups, which are often used for targeting purposes, must be specifically installed at the end of the hydrophilic terminus.[31,32] By extension of this feature, for installing few different surface functionalities, polymers with these different terminal functional groups must be independently synthesized and co-assembled.[31, 32]

In addition to size and surface functionalization features, these supramolecular assemblies also must exhibit excellent host-guest characteristics. For example, most cancer chemotherapeutic molecules are highly toxic. Therefore, it is essential that drug molecules are stably encapsulated within the interiors of these vehicles to prevent premature release of drug molecules, when these systems undergo large dilution during biodistribution and when interacting with biological components such as cellular membranes and serum proteins that can competitively sequester these molecules to cause off-target release. [33-35] A consequence of stable encapsulation is that these nanoassemblies must be programmed to release their hydrophobic guest molecules in the presence of a bio-relevant trigger, such as a biomarker for a disease so that the drug molecules are released at the location of a specific lesion.[12, 36] The intrinsic instability of the micelles under diluted conditions will cause the disassembly and premature release of the drug molecules especially under complex serum condition. Therefore, it is difficult to achieve high encapsulation stability for the block copolymer micelle.[34, 35, 37-39] For instance, the widely used PEG-PDLLA block polymer micelle has been found to rapidly release the encapsulated hydrophobic agents during circulation under *in*

vivo conditions.[40] Even the polyethylene glycol-phospholipid micelles with enhanced stability were proposed, however, the nanoparticles can only be stable for 1-2 h under serum conditions.[41] Even though the increased polymeric hydrophobicity of the micelle may enhance the encapsulation, the encapsulated drug would lack efficient release mechanism in these cases.[34,36]

Recent molecular design strategies can overcome one or more of these barriers to increase the chemotherapy efficiency.[42-45] For instance, layer-by-layer approaches have been used to prepare assemblies with tailorable crosslinking-based stabilization and surface functionalization features. [46] Similarly, shell crosslinked micelles have been developed for enhancement of the carrier stability and facile surface engineering. [47] Nonetheless, fulfilling all these structural and functional requirements, mentioned above, in a single system continues to be a challenge.

Moreover, introducing functional groups in nanoparticles often involve multiple and often tedious steps. Multi-component reactions (MCRs), involving three or more starting materials performed in one pot for the preparation of a single final product, have been of interest for their atom economy and efficiency. [48-53] MCRs were initially developed for the synthesis of small molecules and have been launched for the preparation of large libraries of molecules with the diversity and complexity that are critical for drug development and screenning. [51-53] More recently, these strategies have been brought to bear for the synthesis of polymers with different topologies, structures, architectures and properties. [54-60] However, to our knowledge, MCRs have not been exploited for the preparation of advanced nanostructures such as hierarchical polymeric assemblies with tailorable properties. In this paper, we use an efficient one-pot multicomponent sequential reaction for the preparation of the complex supramolecular nanoassemblies with tunable features desired in a therapeutic delivery vehicle, where the surface functionalization and crosslinking-based stabilization of nanocarrier are achieved simultaneously in one-pot with water as the solvent.

Our approach to prepare nanoparticles and its features that highlight the key advantages in drug delivery applications include the fact that: (*i*) the synthetic procedure is simple to perform multistep reaction for nanoparticles in one pot, which is beneficial for scalability; (*ii*) the reaction is performed with high atomic efficiency in a green solvent, water; (*iii*) the NPs exhibit high encapsulation stability because of their crosslinked nature; (*iv*) the NPs are triggerable for molecular release, as the crosslinks are based on disulfide bonds that are susceptible to the reducing intracellular conditions [61]; and (*v*) the nature of the self-assembly process and the multi-component feature allows for an unprecedented and convenient tunability in size, hydrophobicity of the interior, and surface functionalities. We elaborate the details of our preliminary findings and details in this paper.

RESULTS AND DISCUSSION

Three component sequential reaction for nanoparticles with controllable sizes

Simple synthetic procedure to prepare the NPs, while offering the flexibility in endowing them with functional characteristics, is the key for a scalable impact. Cascade chemical reactions in a single pot offer that unique opportunity. The three-component sequential reaction that is used in the formation of the nanoassembly involves two reactions, where the reactive functionality for the second step is generated in the first step and the functional groups involved in the first and the second step are mutually compatible. The molecular design that offers this possibility is shown as **P1** in Fig. 1. We note here that the synthesis of the random copolymer itself requires much lower levels of synthetic efforts, compared to the block copolymer, which is good for scale up.[22-24] This random copolymer contains a hydrophilic polyethyleneglycol (PEG) methacrylate and two different hydrophobic methacrylate monomers containing an amine-reactive γ-thiolactone unit and a thiol-reactive pyridyldisulfide unit. In this case, an externally added amine (R-NH_2) would specifically react with the γ-thiolactone unit to cause a ring opening of the

latter to reveal a thiol moiety. This thiol moiety would then react with the pyridyldisulfide moiety to generate disulfide bonds. We hypothesized that in a polar environment, this random copolymer would self-assemble into a nanoscale structure, which can be captured using the three-component reaction induced crosslinking process. The initial amide bond formation using the substituted primary amine allows for incorporation of variations in the functional groups present within the interior of the polymer assembly, as well as on the surface of the nanoparticles (Fig. 1). The ring opening and the disulfide bond formation reactions provide the crosslinking required for the formation of the nanoparticle. Moreover, if the crosslinking process occurs exclusively within the initially formed aggregate, *i.e.* without any crosstalk among the nanoassemblies, then the ability to achieve variations in noncovalent supramolecular assemblies would directly offer access to various crosslinked nanoparticles.

The thiolactone-containing monomer synthesis started with the reaction of DL-homocysteine thiolactone hydrochloride with succinic anhydride in the presence of sodium bicarbonate. The resultant carboxylic acid moiety was coupled to hydroxyethylmethacrylate (HEMA) monomer under EDC-coupling conditions to obtain the targeted monomer (see Supporting Information for details). Note that the amine moiety of the starting material could indeed be directly coupled with methacrylic acid to obtain a monomer with the thiolactone on the side chain. However, the solubility of this monomer was not compatible for copolymerization with other monomers in this reaction. Polymer **P1** was obtained through copolymerization of the thiolactone monomer above with PEG-methacrylate and pyridyldisulfidyl-ethyl-methacrylate monomers under RAFT polymerization conditions. To label the polymer **P2**, a **P1** analog with a fluorophore label, these three monomers were copolymerized with a small percentage of an additional monomer containing rhodamine b. Synthetic and characterization details for the monomers and the polymers are described in the Supporting Information. Molecular weight (M_n) of **P1** is ~14 k with a dispersity of 1.1. The ratio of the chemical compositions (PEG: thiolactone (TLt): pyridyldisulfide (PDS))

was found to be about 30: 35: 35 based on the NMR integration of their characteristic peaks respectively at 3.37, 4.61, 8.46 ppm (Fig. S7). The dye labeled polymer (**P2**) has almost the same composition with ~1% of rhodamine b label.

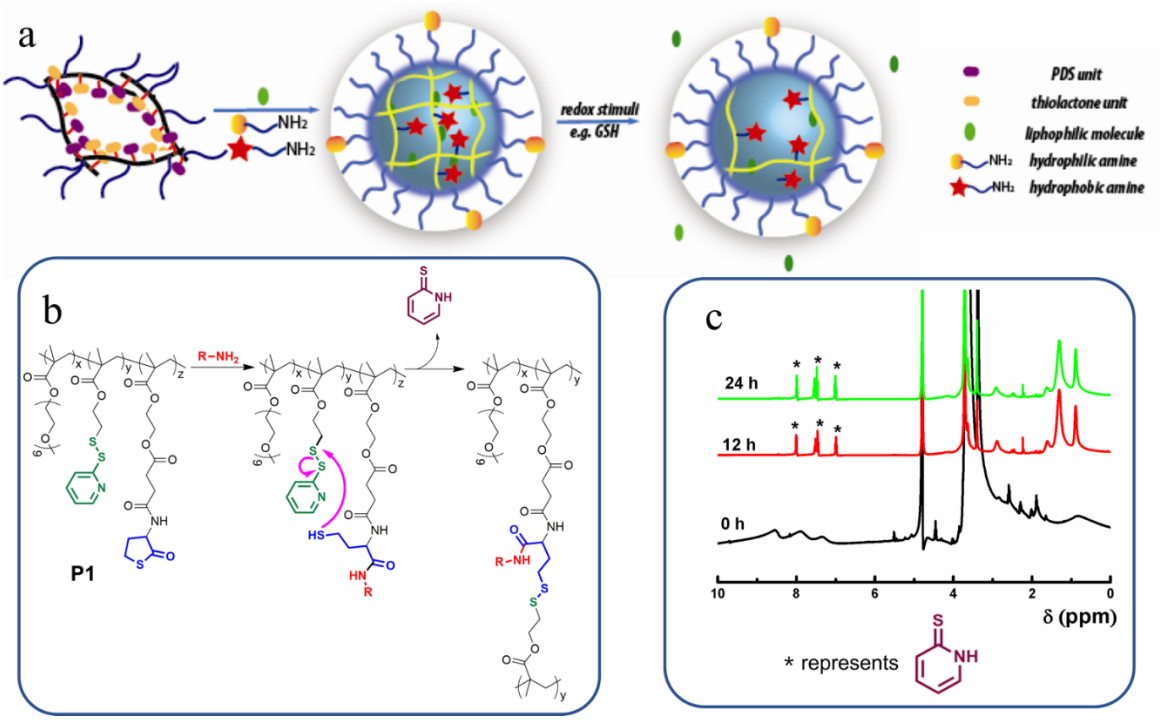

Fig. 1. a) Schematic illustration of preparation of the nanoparticles and the responsive release process; b) the chemical transformation of 3-component sequential reaction for nanoparticles; c) NMR spectra for monitoring the 3-component sequential reaction process in D_2O. The stars represent the byproduct of pyridinethiol from the reaction as the readout.

The next step is to use this polymer precursor to test the idea of using the three-components sequential reaction to prepare crosslinked polymeric nanoparticles. To qualitatively assess whether the amphiphilic random copolymer forms assemblies in aqueous phase, ^{1}H NMR of **P1** was assessed in D_2O. Indeed, the aromatic peaks that correspond to the PDS units in the polymer were found to be very broad (Figure 1c), relative to the same polymer in an organic solvent (see SI). This observation was taken to indicate the formation of a nanoscale aggregate in aqueous phase, where the PDS units are mostly buried within the interior of the assembly with limited segmental mobility. Upon of addition of one equivalent of octylamine, there was a clear emergence of sharp aromatic NMR peaks that are attributed to the formation of the

pyridothione byproduct of the anticipated three-component reaction.

The reaction was deemed efficient as all the PDS groups in the polymer aggregate seem to have been transformed to the pyridothione within 12 h even at low reactant concentrations. For comparison, when the same three-components reaction was also performed in an organic solvent, where there is no self-assembly is anticipated, the reaction was found to be much slower (Fig. S18). This is understood as the hydrophobicity driven nanoaggregate formation in water would significantly increase the local concentration of the reactively complementary moieties.

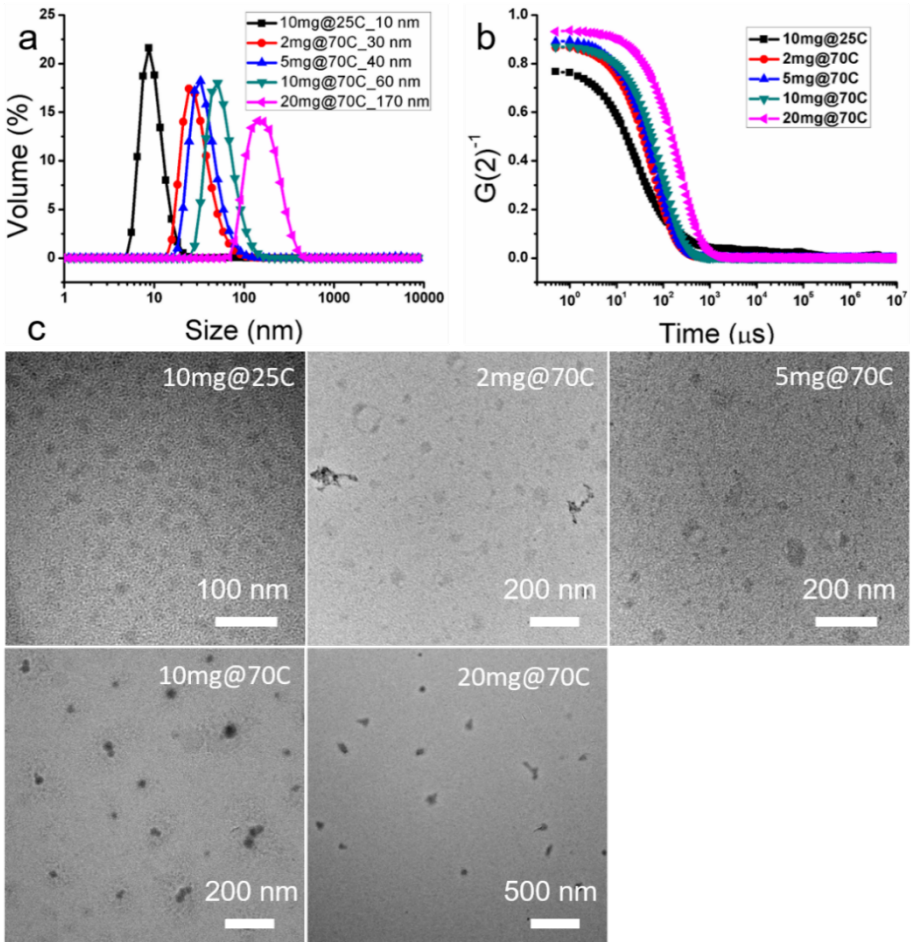

Fig. 2. Size control of the nanoparticles. a) size of the nanoparticles by DLS from different preparation methods (measurements were performed at 25 °C). The size of the nanoparticles was varied from 10 nm to 30 nm, 40 nm, 60 nm and 170 nm. b) correlation function of the nanoparticles from DLS. All the nanoparticles exhibited good correlation functions. c) unstained TEM images of corresponding nanoparticles with different sizes from different preparation methods. The names present the preparation conditions for different nanoparticles. For example, 10mg@70C means the nanoparticles prepared with 10 mg polymer in 1 mL water at 70 °C.

Next, we were interested in controlling the properties of the nanoparticles, specifically their size. The

ability to vary size of the nanoparticles was motivated by the fact that the impact of nanoassemblies in many biological applications, such as drug delivery, is dictated by size. [25] These precise size requirements do also vary with different disease models. [62] Therefore, an ideal nanoscale platform would allow control over size of the nanoparticles. To this end, we attempted to vary the self-assembly conditions that would offer variations in the size of the nanoassemblies. When **P1** was assembled in water at 10 mg/mL concentration, the resultant aggregate was found to be ~15 nm at room temperature (Fig. S19). When this aggregate was crosslinked at ambient temperature with hexylamine, the polymer nanoparticle was found to be ~10 nm, suggesting that the intermolecular crosslinking process could cause collapse of the aggregate (Fig. 2a). We explored the possibility of utilizing the propensity of PEG-based polymers to exhibit variations in aggregate sizes, because of their temperature-dependent dehydration possibilities. [63, 64] Indeed, as we increased the temperature to 70 °C, the size of the aggregates increased, which was also found to exhibit a systematic dependence on the concentration of the polymer. With this observation, we were able to tune the size of the nanoparticles over a broad range from 30 nm to 40 nm, 60 nm, 170 nm or even ~1000 nm using polymer concentrations of 2 to 5, 10, 20 and 30 mg/mL (Fig. 2 and Fig. S21), when the crosslinking reaction was carried out at 70 °C.

Size of these nanoparticles were mainly determined by dynamic light scattering, where all assemblies exhibited excellent correlation function. Although these particles were formed at 70 °C, DLS measurements were performed at ~25 °C, where the initial assemblies were found to be substantially smaller. The fact that the sizes of the crosslinked assemblies did not change at 70 °C (Fig. S21c), which suggest that the crosslinking process can efficiently lock the size of the nanoparticles. The nanoparticles were also characterized using transmission electron microscopy (TEM), as shown in Fig. 2. The nanoparticles were spherical and exhibited a slight decrease in size, relative to that from DLS measurements, suggesting that these soft nanoparticles collapse in dry state. Finally, it is noteworthy that all these nanoparticles were found

to be stable in water for long periods of over a month (Fig. S22).

Functionalization of the nanoparticles

Functionalization of the NPs affords us the opportunity to tune the properties for a wide range of applications. A key feature of the three-component sequential reaction here is that the primary amine, used as the initiating reactant of the reaction cascade, offers the opportunity to incorporate diverse functionalities on the nanoparticle surface. To this end, we systematically varied the alkyl group in the alkylamine, R-NH_2. Accordingly, we initiated the crosslinking reaction with alkyl moieties containing a negatively charged carboxylic acid moiety or a positively charged quaternary ammonium group, along with a control that does not bear any charge (hexylamine). The charged nature of the first two functionalities should dictate the surface charge of the nanoparticle, which was assessed with zeta potential measurements (Fig. 3). The surface charge of the functionalized particles was indeed found to be negative (-42.8 eV) for the carboxylic acid functionalized nanoparticle, while the ammonium functionalized nanoparticle exhibited a positively charged surface (+11.4 eV). Interestingly, the hexylamine-functionalized control nanoparticles was found to be negatively charged, albeit with a lower magnitude. This observation is however consistent with other PEG-functionalized nanoparticles reported in the literature. [65]

A reasonable expectation, among these structural variations, is that the surface exposure of the modifying functionalities would be dictated by their solvophobicity. Thus, when the modification is based on a hydrophilic functionality, these functionalities would be mostly presented on the exterior of the nanoparticle. Conversely, the hydrophobic moieties would mainly become part of the core of the nanoparticle. While the zeta potential measurements support this hypothesis for the positively and negatively charged nanoparticles, we further explored the hydrophobic modifications with pyrenemethylamine, a spectroscopic probe. The absorption and emission spectra of this modification are shown in Fig. S23 and Fig. 3d, respectively. The characteristic absorption peak for pyrene showed the

functionalization of the nanoparticle with the pyrene functionality. On the other hand, the presence of the excimer emission peak along with the monomer emission peak in the fluorescence spectrum suggests that these functionalities are most likely present within the interior of the nanoparticle. To further explore whether these excimer peaks are due to an aggregation of surface exposed pyrene moieties, the nanoparticle solution was diluted by about 20 times and the excimer emission peak is still seen. These data further support the idea that the hydrophobic modifications mostly affect the interior of the nanoparticle. This feature has implications in the host-guest properties of these nanoparticles, which we explored further (*vide infra*).

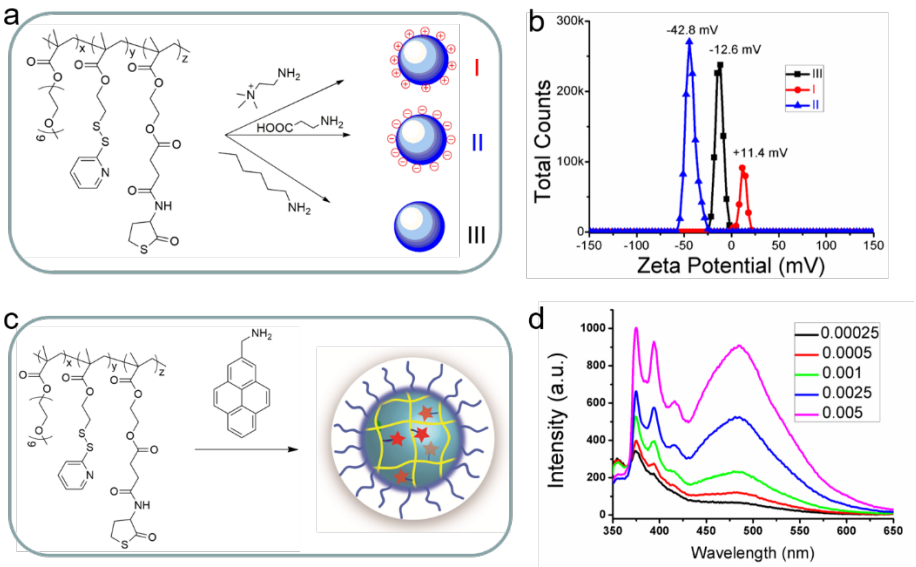

Fig. 3. Functionalization of the nanoparticles. a and b) functionalization of the nanoparticles with different charged species on the surface. a) chemical illustration of the functionalization, b) zeta-potential of the nanoparticles; c and d) interior functionalization. c) chemical illustration, d) emission spectra of the nanoparticles with different concentrations (unit: mg/mL).

In order to demonstrate the utility of the facile surface functionalization capabilities, we targeted the decoration of the nanoparticles with functionalities that can specifically target a sub-cellular compartment in a cell. Prior to carrying out any cellular experiments, it is imperative that we test whether these nanoparticles are cytotoxic, as this might preclude any meaningful sub-cellular targeting. Accordingly,

toxicity of the nanoparticles was assessed using an MTT assay. The nanoparticles did not exhibit any discernible cytotoxicity, even at a concentration of 0.2 mg/mL (Fig. 4a). The data shown in Figure 4a are based on 60 nm nanoparticles. To assess whether size variations have any effect on the cytotoxicity, nanoparticles of different sizes were assessed and were also found to be non-toxic (Fig. S25). To even further test these nanoparticles, the cytotoxicity of the 60 nm nanoparticles was also studied in two more cell lines, MDA-MB-231 and MCF-7 (Fig. 4b and 4c). Here too, the nanoparticles were found to be quite cyto-compatible. A potential issue with a typical cytotoxicity analyses is that a nanoparticle might be deemed non-toxic, because it never was taken up by the cell and thus does not induce any toxicity. To test this possibility, we tested whether the nanoparticles are taken up by the cells using rhodamine B-labeled nanoparticles (Fig. 4d-f and Fig. S26-28). The presence of the bright red color, from the covalently-attached rhodamine B, throughout the cells indicate that these nanoparticles are taken up by the cells after a short incubation time of 4 h. This feature too was found to be true for MDA-MB231 and MCF-7 cell lines (Fig. 4e and 4f) and for nanoparticles of different sizes (Fig. S27 and S28).

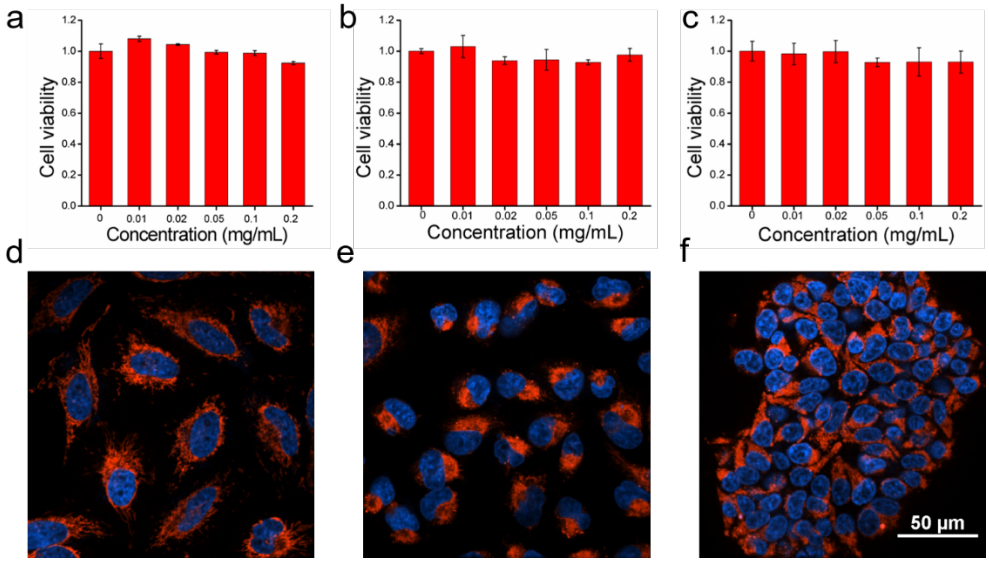

Fig. 4. Cytotoxicity (a, b and c) and cell uptake (d, e and f) of the nanoparticles (size: 60 nm). a and d) HeLa cell; b and e) MDA-MB-231 cell; c and f) MCF-7 cell. The cytotoxicity was performed by MTT assay. The confocal images were recorded after 4 h incubation with the concentration of 30 µg/mL of nanoparticles. The red color represents the Rhodamine b dye labelled NGs. The blue color represents the nucleus after hoechst 33342 staining.

To investigate the possibility of sub-cellular targeting using functionalities presented on the surface of the polymer nanoparticles, triphenylalkylphosphonium moieties were incorporated on the surface of the nanoparticles, as these functionalities are known to target mitochondria. Structure of the polymeric nanoparticle is shown in Fig. 5. Synthetic and characterization details of the ligand molecules and their incorporation on the surface of the nanoparticles are detailed in Supporting Information. The intracellular distribution of the nanoparticles and the potential mitochondrial targeting was studied using a high-resolution confocal microscope. In this experiment, the mitochondria were stained with a green mitotracker dye. Nanoparticle localization in the mitochondria was then assessed by evaluating the colocalization of the green color from this dye with the red color of the rhodamine-labeled nanoparticle. As shown in Fig. 5, the triphenylalkylphosphonium-decorated nanoparticles exhibited excellent mitochondrial localization, while the unfunctionalized nanoparticle exhibited no localization in the mitochondria (Fig. 5b). The ability to deliver nanoparticles to specific sub-cellular organelle offers many opportunities for improving therapeutic approaches through targeting. [66]

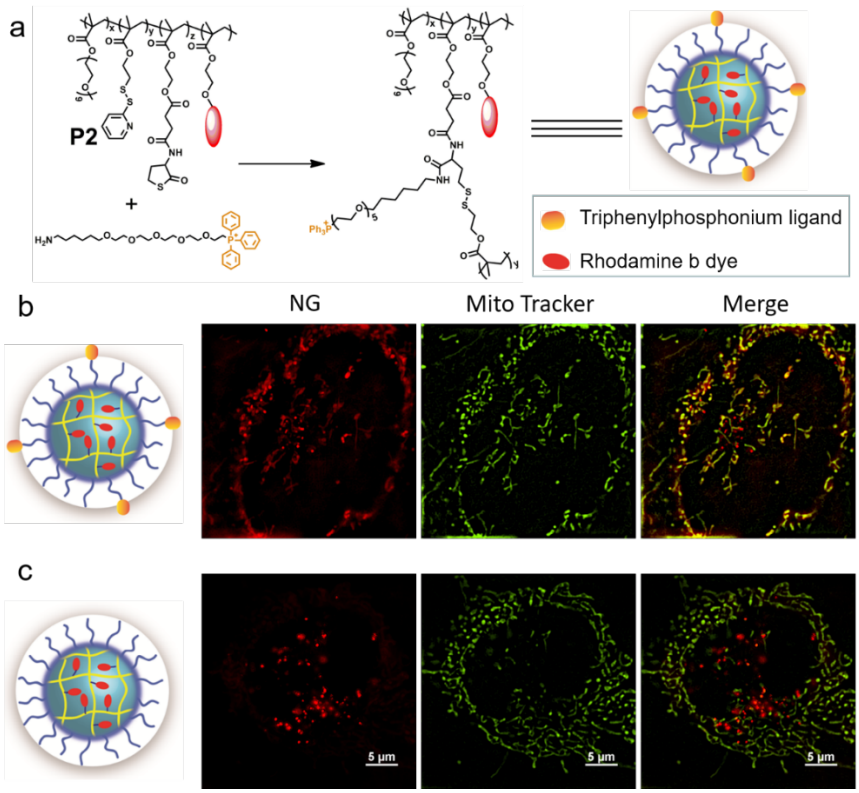

Fig. 5. Mitochondria targeting experiment. The SIMe images of nanoparticles uptake by HeLa cell after 4 h incubation. a) ligand functionalized nanoparticles, b) control nanoparticles without ligand.

Non-covalent encapsulation and triggered release of guest molecules

Stable encapsulation of the guest molecules with a triggerable release modality is the key feature to ultimately implement these NPs in practical applications. In addition to the surface functionalization, we also surmised that when modified with hydrophobic amines, the interior of these nanoparticles would be affected. To test this idea further, we tested the noncovalent encapsulation capability of the nanoparticles. Accordingly, we systematically varied the hydrophobicity of the modifying functionality in the nanoparticle using hexylamine, octylamine, decylamine, and benzylamine. The ability of these nanoparticles to non-covalently bind to guest molecules was assessed using Nile red as the probe. All nanoparticles exhibited the ability to non-covalently bind the spectroscopic probe, where the extent of guest loading inside the nanoparticles seemed to depend on the functional group. Interestingly, octylamine modified nanoparticles exhibit the optimal ability to bind Nile red, compared to both hexylamine and decylamine (Fig. S24). These results could be rationalized by the possibility that there is a balance between the hydrophobicity of the modifying functionality and its sterics-induced volume exclusion.

An equally important criterion for a good host, especially in the context of a drug carrier, involves the encapsulation stability of the guest molecule in the nanoparticle. The encapsulation stability of the nanoparticle for hydrophobic guest molecules should directly correlate with the hydrophobicity of the modifying amine functionality. We used the previously developed fluorescence resonance energy transfer (FRET) based method [67] to evaluate the encapsulation stability of the nanoparticles. Briefly, a solution containing a FRET donor molecule as the guest in the nanoparticle host is mixed with a similar solution with the corresponding FRET acceptor molecule as the guest. The kinetics of FRET evolution provides direct insights into the encapsulation stability; faster FRET evolution indicates poor encapsulation stability.

Hydrophobic cyanine dyes, DiO and DiI, were used as the FRET donor and acceptor molecules respectively for this study. First the encapsulation stability of the amphiphilic polymer assembly, before crosslinking was assessed as the control. The non-crosslinked polymeric nanoaggregate showed very fast FRET increase rate with a rapid increase of the acceptor emission at 550 nm and decrease of the donor emission at 510 nm (Fig. 6a), with a leakage coefficient of >18/h, suggesting a leaky nanoaggregate. Next, the crosslinked nanoparticles based on reaction with hexylamine was evaluated. Here too, there was a temporal evolution of the FRET ratio, however the evolution was found to be much slower with a leakage coefficient of 4.57×10^{-3}/h (Fig. 6c and Fig. S29). As the hydrophobicity of the amine increases from the hexylamine to octylamine and decylamine based nanoparticles, the encapsulation stability substantially increased with no discernible temporal evolution of FRET for the latter two nanoparticles (Fig. 6e and 6g). The alkylamine-induced crosslinking reaction can provide enhanced encapsulation stability due to two different reasons – enhanced hydrophobicity of the interior endowed by the incorporation of the alkyl moiety and the crosslinking of the interior that offers increased steric barrier for molecular diffusion out of the nanoparticles. The increased encapsulation stability with increasing hydrophobicity of the alkyl chain suggests that the former is certainly a factor. To test if there is contribution from the latter, the nanoparticle crosslinking was initiated using a hydrophilic polyethyleneglycol-amine (PEG_8-amine). The resultant nanoparticle exhibited better encapsulation stability, compared to the uncrosslinked control nanoaggregate, with a leakage coefficient of ~4.2/h. However, this encapsulation is much poorer compared to that from the hexylamine. These results clearly show that both crosslinking based steric barrier and hydrophobicity based encapsulation play critical roles in the encapsulation stability in these nanoparticles.

If these nanoparticles were to be useful, it is also essential that this stable encapsulation is compromised in the presence of a specific biologically relevant trigger. Because of the presence of the disulfide bonds, these are likely to be susceptible to the presence of a reducing agent such as dithiothreitol (DTT). Indeed,

the FRET evolution was found to be significant faster in the presence of mM concentration of DTT (Fig. 6d and Fig. S30). Interestingly however, no change in FRET evolution was observed for octylamine and decylamine based nanoparticles even in the presence of DTT (Fig. 6f and 6h). The main reason is the increase in the hydrophobicity to stabilize the NPs under pure water solution. When we use serum as the medium (*vidfe infra*), the dye can still be released out from the NPs in the presence of DTT. Based on the results, we conclude that crosslinking can efficiently enhance the stability of the nanoparticles.

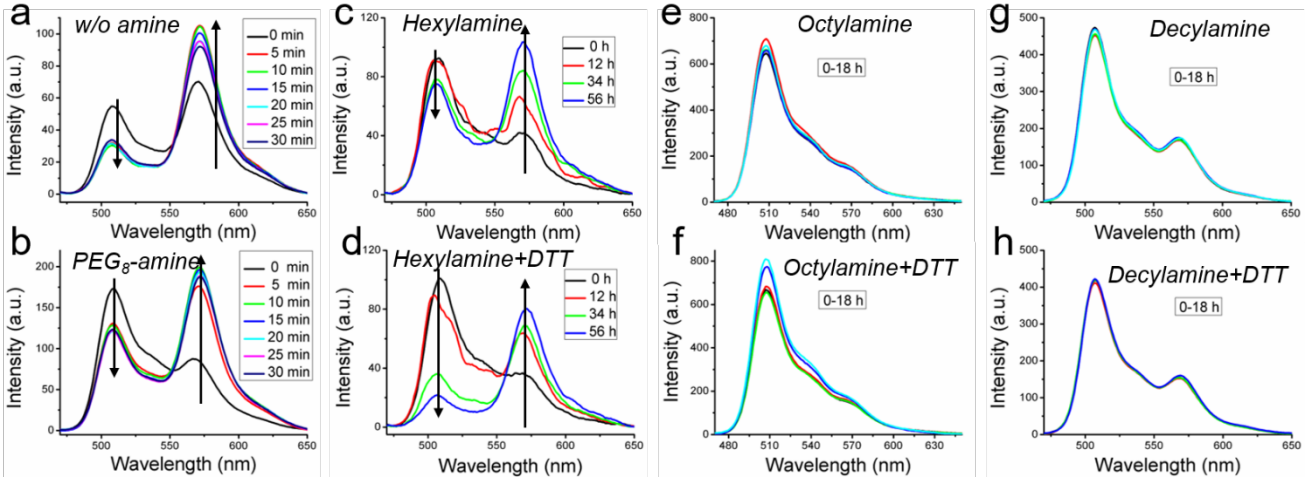

Fig. 6. FRET experiment of nanoparticles from different amines. a) no amine, b) PEG_8-amine, c and d) hexylamine, e and f) octylamine, g and h) decylamine. a, b, c, e and g) in the absence of DTT; d, f, h) in the presence of 10 mM DTT. The fluorescent spectra were measured by excitation wavelength at 450 nm.

The studies above show that the encapsulation stability in these nanoparticles is dependent on the hydrophobicity of the modifying functionalities and the crosslinks in the nanoparticle in aqueous solution. An even more rigorous study of the encapsulation stability in the context of biological applications would involve evaluating it under serum conditions. We adapted a previously reported method [68] for this purpose, where the FRET pairs are co-encapsulated in the nanoparticle. In this case, the solution already exhibits excellent FRET (Fig. S31). If the encapsulation stability is poor, the hydrophobic guests would leave the interior of the nanoparticle and accumulate in the reservoir offered by the serum proteins that are capable

of binding to hydrophobic molecules, such as serum albumin. Interestingly, the leakage coefficient of the uncrosslinked nanoaggregates and the hexylamine-based nanoparticles was found to be higher in serum (Fig. 7). Here too, the octyl- and the decyl- nanoparticles were still found to exhibit stable encapsulation. However, when the experiments were performed in the presence of 10 mM DTT, even the octylamine and decylamine based nanoparticles exhibited a lower FRET ratio over time, as discerned by the increase of the donor peak and decrease of the acceptor emission peak (Fig. 7f and 7h). These results also show that our strategy can efficiently endow the particles with high encapsulation stability without any leakage of the guest molecules under serum conditions. On the other hand, there have been recent reports that show that micelles based on many block copolymers can stably encapsulate hydrophobic molecules in water, but exhibit fast leakage under serum conditions at the time scales used in the present work.[38-41] These results also highlight that encapsulation stability in water is not a sufficient measure for evaluating nanoparticles for biological applications such as targeted drug delivery.

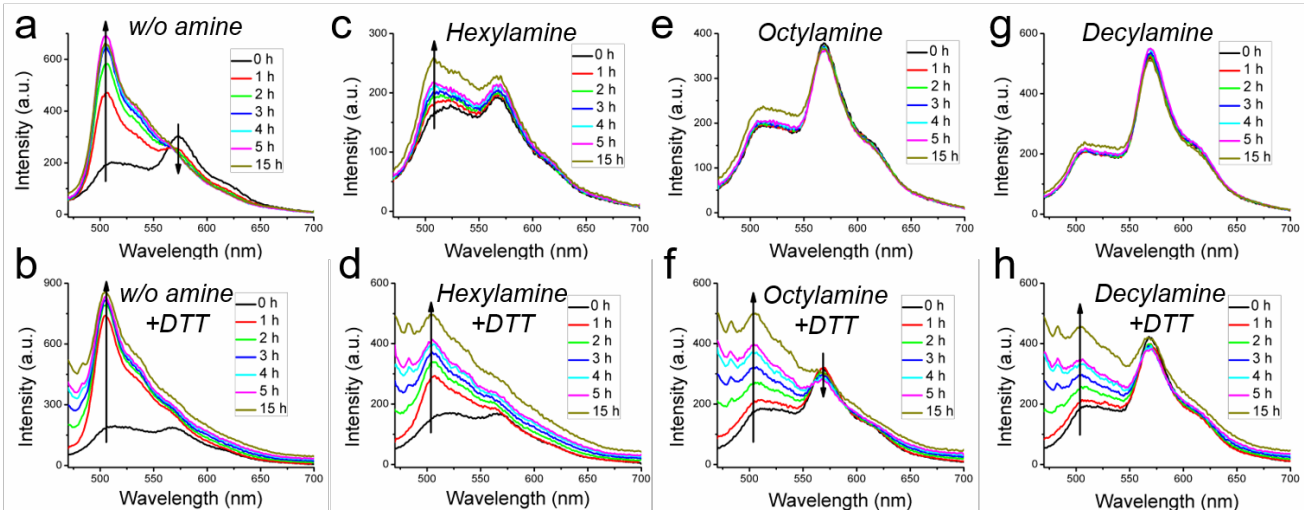

Fig. 7. Serum stability test toward nanoparticles prepared from different amines. All the FRET experiments were performed in serum (90%). a and b) no amine, c and d) hexylamine, e and f) octylamine, g and h) decylamine. a, c, e and g) in the absence of DTT; b, d, f, h) in the presence of 10 mM DTT. The fluorescent spectra were measured by excitation wavelength at 450 nm.

Next, we evaluated whether the observed trend in encapsulation stability translated to molecular release

kinetics variations inside cells, as the cytosolic environments of most cells are highly reducing. If we were to use the encapsulated FRET pairs, we might not be able to discern the difference between cellular uptake followed by molecular release and leakage of molecules outside the cells where the hydrophobic molecules can then passively diffuse inside the cells. To circumvent this, the nanoparticles were covalently labeled with rhodamine B, which can act as the FRET acceptor for the donor dye DiO. The latter was non-covalently encapsulated as the hydrophobic guest molecules within the nanoparticles (Fig. S32). The principle of this method is similar to the experiments in the serum, where there would be a high FRET because of the concurrent presence of both the donor and the acceptor in the nanoparticle. However, if the non-covalently encapsulated molecules were to be released, then the decreased proximity between these molecules will substantially impact the FRET. We used the spin disk fluorescent microscopy and A1R spectral microscope to study the encapsulation stability in HeLa cells after 4 h and 24 h incubation times. As the donor DiO is a green dye, we used the 488 nm laser for excitation. Two different filters were monitored for emission: the 505-525 nm channel present the DiO emission and the 585-605 nm channel present the rhodamine B acceptor emission (Fig. S33 and Fig. 8). The relative intensity of the green channel and the red channel, which also dictates the color in the merged channel, provides insights into the relative kinetics of molecular release from the nanoparticles. For the non-crosslinked nanoaggregate, there is a significant emission from the green channel and the merged image is quite green, suggesting that the DiO guest molecule has been released from the nanoparticle. The hexylamine based nanoparticle shows a mixture of the green and fluorescence in the merged image indicating slow release of the guest molecule, while the domination of the red fluorescence in the decylamine nanoparticle suggests high encapsulation stability with very little to no molecular release in 24 hours.

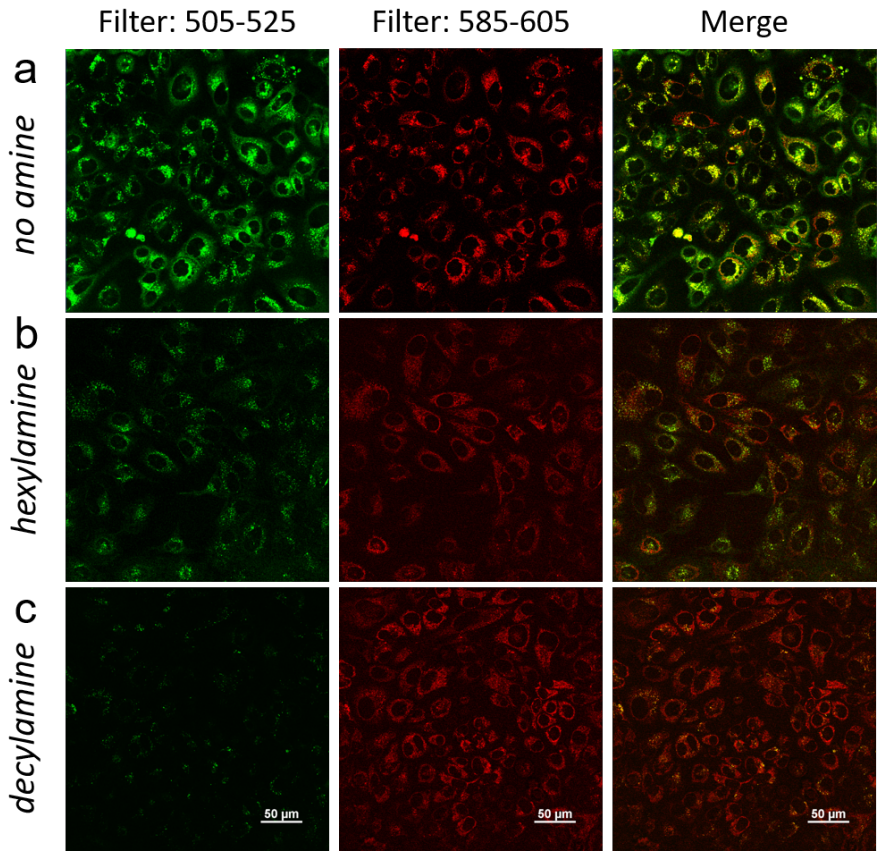

Fig. 8. FRET experiment toward different nanoparticles from different amines (a, no amine; b, hexylamine; c, decylamine) inside cells (HeLa cell line) after 24 h incubation. The confocal image was recorded by excitation wavelength of 488 nm and the images was obtained with two different filters in the range of 505-525 nm and 585-605 nm.

To more quantitatively compare the encapsulation stability inside cells, we used spectral confocal microscopy to obtain the emission spectra inside the cells. Three different nanocarriers (non-crosslinked nanoaggregate, hexylamine functionalized nanoparticles and decylamine functionalized nanoparticles) were studied by cell uptake after 24 h incubation (Fig. 9). There is very little FRET in the cells (FRET ratio $I_a/(I_a+I_d)=0.26$) for non-crosslinked nanoaggregates, which is attributed to the possible release of the guest molecules even prior to cellular uptake. After the hydrophobic functionalization of the nanoparticles with hexylamine to decylamine, the FRET ratio was found to be a much higher with values of 0.49 and 0.62.

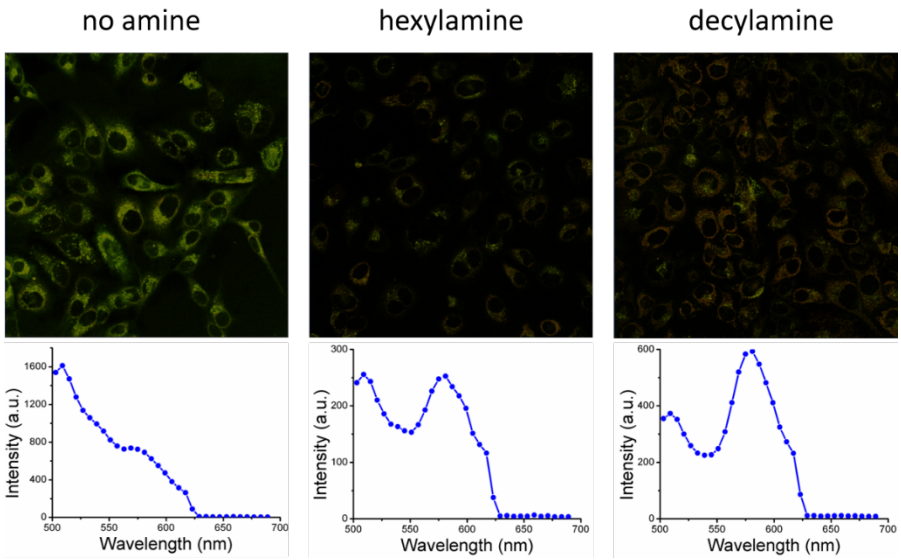

Fig. 9. In cell FRET study of different nanoparticles from different amines (no amine, hexylamine, decylamine). The images and spectra were obtained from the spectral confocal microscope with excitation wavelength at 488 nm after 24 h incubation.

To further assess whether there is a time-dependent intracellular release of the guest molecules, the FRET ratio was monitored for the hexylamine-based nanoparticles at 4, 27, and 51 hours. As shown in Fig. 10, the emission at ~560 nm deceased, with a concurrent increase in the emission at ~510 nm. This change corresponded to the FRET ratios 0.68, 0.47 and 0.33 at 4, 27, and 51 hours respectively. Moreover, the site selected spectra obtained from inside the cells also showed similar results (Fig. 10 d, h and l). These results clearly show that the intracellular reducing environment of the cells, due to high glutathione concentration, can cause molecular release inside cells, the rate of which is correlated with the encapsulation stability obtained in test tube experiments.

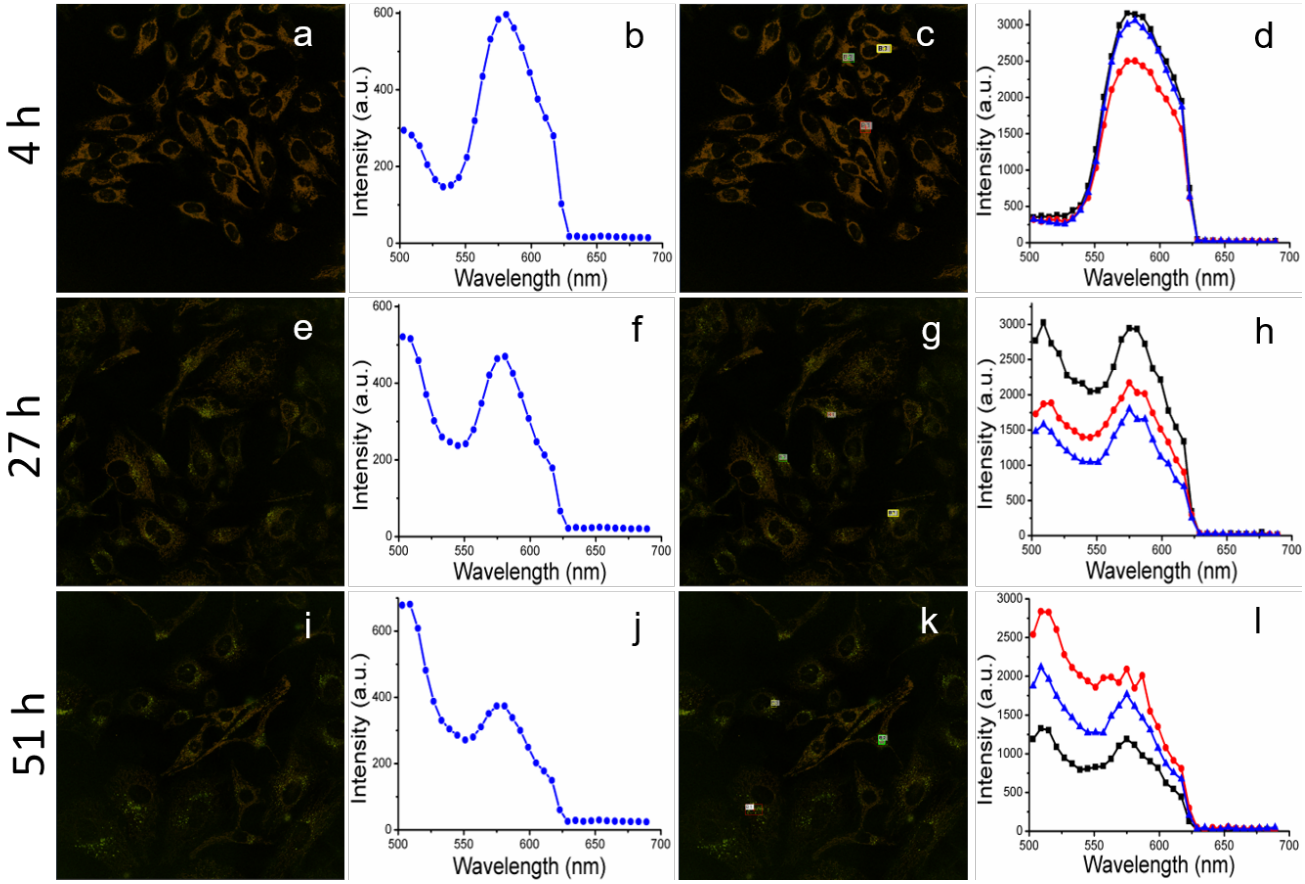

Fig. 10. Time dependent in-cell FRET study of nanoparticles (from hexylamine). The images and spectra were obtained from the spectral confocal microscope with excitation wavelength at 488 nm after different time incubation (4 h, 27 h and 51 h). a, e, f, c, g, k are the spectral images. b, f and j are the emission spectra from a, e, and I respectively. d, h and j are the emission spectra from the selected area in c, g and k respectively.

As the nanoparticles exhibit many tunable features that are translatable to inside cells, we carried out preliminary experiments to assess the possibility of these nanoparticles acting as a carrier for chemotherapeutic drug molecules to be released under intracellular conditions. We used camptothecin (CPT) because of its hydrophobicity and well-established pharmacology. A ~60 nm hexylamine-based nanoparticle was synthesized with 13% loading capacity (1.3 mg drug/10 mg polymer) of the drug (Fig. 11b and Fig. S34). Cell viabilities were then evaluated at different concentrations of CPT-loaded nanoparticles in three different cancer cells (HeLa, MDA-MB-231, MCF-7). The extent of cell death was investigated after different times (24 h, 48 h and 72 h). The cell death efficiency was comparable with the free drug in most cases for the nanoparticle and was even better in some cases suggesting that the

nanoparticle is capable of making the hydrophobic drug molecule more bioavailable.

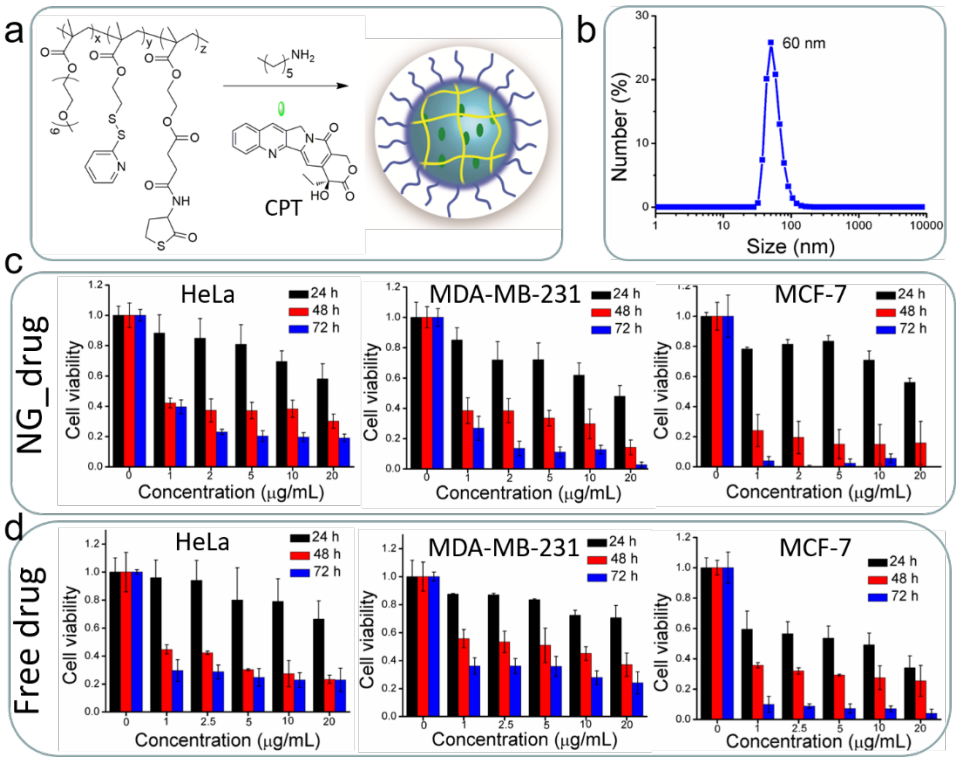

Fig. 11. Cytotoxicity of the drug loaded nanoparticles. a) process for drug loaded nanoparticles, b) DLS of CPT loaded nanoparticles, c) concentration and time dependent cytotoxicity of the drug loaded nanoparticles, d) cytotoxicity of the free drug.

CONCLUSIONS

A facile strategy for the preparation of nanoparticles with tailorable properties through concurrent functionalization and stabilization has been demonstrated using a sequential three-component reaction. By tuning the polymeric structure and self-assembly conditions, we have shown that the non-covalent assembly and thus the resultant nanoparticle sizes can be conveniently tuned by two orders of magnitude. Similarly, the functionalization of the nanoparticles can be used to decorate the outer shell of the nanoparticle to tune its interfacial interaction or to functionalize the interior to optimize its host-guest properties. The former feature has been used to vary the surface charge of the nanoparticles and to target specific organelles in cells. The latter option has been exploited to evaluate variations in the hydrophobicity

that offer an optimal encapsulation stability, where the guest molecules are robustly encapsulated in one set of conditions but are reliably released in a target environment. Three different FRET-based methods, including an in-cell FRET experiment, have been used to test the effect of core structure variations upon encapsulation stability in aqueous solutions, in serum and inside cells. The ability to tightly tune the physiochemical properties of nanoparticles has implications in a variety of applications, including in drug delivery and diagnostics. As a preliminary demonstration, we have shown that these nanoparticles can encapsulate hydrophobic drug molecules and can be released in the target intracellular environment with high fidelity.

ASSOCIATED CONTENT

Supporting Information. Materials & methods for synthesis and characterization of polymers, nanoparticles preparation, procedures for cellular studies.

AUTHOR INFORMATION

Corresponding Author

*thai@chem.umass.edu

Notes

The authors declare no competing financial interest.

ACKNOWLEDGMENTS

We thank the National Science Foundation (CHE-1307118) for support.

REFERENCES

1. Mura, S., Nicolas, J., and Couvreur, P. (2013). Stimuli-Responsive Nanocarriers for Drug Delivery.

Nat. Mater. *12*, 991-1003.

2. Pelaz, B., Alexiou, C., and Alvarez-Puebla, R. A. et al. (2017). Diverse Applications of Nanomedicine. ACS Nano *11*, 2313-2381.

3. Kumari, P., Ghosh, B., and Biswas, S. (2016). Nanocarriers for Cancer-Targeted Drug Delivery. J. Drug Target *24*,179-91.

4. Comoglu, T., Arisoy, S., and Akkus, Z. B. (2017). Nanocarriers for Effective Brain Drug Delivery. Curr. Top. Med. Chem. *17*, 1490-1506.

5. Sun, T., Zhang, Y., Pang, B., Hyun, D. C., Yang, M., and Xia, Y. (2014) Engineered Nanoparticles for Drug Delivery in Cancer Therapy. Angew. Chem. Int. Ed. *53*, 12320-12364.

6. Liong, M., Lu, J., Kovochich, M., Xia, T., Ruehm, S. G., Nel, A. E., Tamanoi, F., and Zink, J. I. (2008). Multifunctional Inorganic Nanoparticles for Imaging, Targeting, and Drug Delivery. ACS Nano *2*, 889-896.

7. Zhao, M., Zen, E., and Zhu, B. (2015). The Biological Applications of Inorganic Nanoparticle Drug Carriers. ChemNanoMat *1*,82-91.

8. Pattni, B. S., Chupin, V. V., and Torchilin, V. P. (2015). New Developments in Liposomal Drug Delivery. Chem. Rev. *115*, 10938-10966.

9. Madaan, K., Kumar, S., Poonia, N., Lather, V., and Pandita, D. (2014). Dendrimers in Drug Delivery and Targeting: Drug-Dendrimer Interactions and Toxicity Issues. J. Pharm. Bioallied Sci. *6*, 139-150.

10. Uhrich, K. E., Cannizzaro, S. M., Langer, R. S., and Shakesheff, K. M. (2017). Polymeric Systems for Controlled Drug Release. Chem. Rev. *99*, 3181-3198.

11. Li, Y., Maciel, D., Rodrigues, J., Shi, X., and Tomás, H. (2015). Biodegradable Polymer Nanogels for Drug/Nucleic Acid Delivery. Chem. Rev. *115*, 8564-8608.

12. Kamaly, N., Yameen, B., Wu, J., and Farokhzad, O. C. (2016). Degradable Controlled-Release Polymers and Polymeric Nanoparticles: Mechanisms of Controlling Drug Release. Chem. Rev. *116*, 2602-2663.

13. Elsabahy, M., Heo, G. S., Lim, S. M., Sun, G., and Wooley, K. L. (2015). Polymeric Nanostructures for Imaging and Therapy. Chem. Rev. *115*, 10967-11011.

14. Kakkar, A., Traverso, G., Farokhzad, O. C., Weissleder, R., and Langer, R. (2017). Evolution of Macromolecular Complexity in Drug Delivery Systems. Nat. Chem. Rev. *1*, 1-17.

15. Li, Y., Wang, Y., Huang, G., and Gao, J. (2018). Cooperativity Principles in Self-Assembled Nanomedicine. Chem. Rev. *118*, 5359-5391.

16. Webber, M. J., and Langer, R. (2017). Drug Delivery by Supramolecular Design. Chem. Soc. Rev. *46*, 6600-6620.

17. Tibbitt, M. W., Dahlman, J. E., and Langer, R. (2016). Emerging Frontiers in Drug Delivery. J. Am. Chem. Soc. *138*, 704-717.

18. Blanco, E., Shen, H., and Ferrari, M. (2015). Principles of Nanoparticle Design for Overcoming Biological Barriers to Drug Delivery. Nat. Biotechnol. *33*, 941-951.

19. Roemeling, C., Jiang, W., Chan, C. K., Weissman, I. L., and Kim, B. Y. S. (2017). Breaking Down the Barriers to Precision Cancer Nanomedicine. Trends in Biotechnology *35*, 159-171.

20. Chen, H., Zhang, W., Zhu, G., Xie, J., and Chen, X. (2017). Rethinking Cancer Nanotheranostics. Nat. Rev. Mater. *2*, 17024.

21. Zhang, X., Jackson, J. K., Burt, H. M. (1996). Development of Amphiphilic Diblock Copolymers as Micellar Carriers of Taxol. Int. J. Pham. *132*, 195-206.

22. Yokoyama, M. (2010). Polymeric Micelles as a New Drug Carrier System and Their Required Considerations for Clinical Trials. Expert Opin. Drug Deliv. *7*, 145-158.

23. Gaucher, G., Dufresne, M., Sant, V. P., Kang, N., Maysinger, D., Leroux, J. (2005). Block Copolymer Micelles: Preparation, Characterization and Application in Drug Delivery. J. Controlled Release *109*, 169-188.

24. Cabral, H., Miyata, K., Osada, K., Kataoka, K. (2018). Block Copolymer Micelles in Nanomedicine Applications. Chem. Rev. *118*, 6844-6892.

25. Torchilin, V. (2011). Tumor Delivery of Macromolecular Drugs Based on the EPR Effect. Adv. Drug Delivery Rev. *63*, 131–135.

26. Waku, T., Matsusaki, M., Kaneko, T., and Akashi, M. (2007). PEG Brush Peptide Nanospheres with Stealth Properties and Chemical Functionality. Macromolecules *40*, 6385-6392.

27. Srinivasarao, M., and Low, P. S. (2017). Ligand-Targeted Drug Delivery. Chem. Rev. *117*, 12133-12164.

28. Zhulina, E. B., Borisov, O. V. (2012). Theory of Block Polymer Micelles: Recent Advances and Current Challenges. Macromolecules *45*, 4429-4440.

29. Milchev, A., Bhattacharya, A., Binder, K. (2001). Formation of Block Copolymer Micelles in Solution: A Monte Carlo Study of Chain Length Dependence. Macromolecules *346*, 1881-1893.

30. Chang, T., Lord, M. S., Bergmann, B., Macmillan, A., Stenzel, M. H. (2014). Size Effects of Self-Assembled Block Copolymer Spherical Micelles and Vesicles on Cellular Uptake in Human Colon Carcinoma Cells. J. Mater. Chem. B *2*, 2883-2891.

31. Hisey, B., Ragogna, P. J., Gillies, E. R. (2017). Phosphonium-Functionalized Polymer Micelles with Intrinsic Antibacterial Activity. Biomacromolecules*183*, 914-923.

32. Licciardi, M., Giammona, G., Du, J., Armes, S. P., Tang, Y., Lewis, A. L. (2006). New Folate-Functionalized Biocompatible Block Copolymer Micelles as Potential Anti-Cancer Drug Delivery Systems. Polymer *47*, 2946-2955.

33. Miller, T., Breyer, S., van Colen, G., Mier, W., Haberkorn, U., Geissler, S., Voss, S., Weigandt, M., and Goepferich, A. (2013). Premature Drug Release of Polymeric Micelles and Its Effects on Tumor Targeting. Int. J. Pharm. *445*, 117-124.

34. Owen, S. C., Chan, D. P. Y., and Shoichet, M. S. (2012). Polymeric Micelle Stability. Nano Today *7*, 53-65.

35. Kim, S., Shi, Y., Kim, J. Y., Park, K., and Cheng, J. X. (2010). Overcoming the Barriers in Micellar Drug Delivery: Loading Efficiency, *in vivo* Stability, and Micelle-Cell Interaction. Expert Opin. Drug Delivery *7*, 49-62.

36. Wong, P. T., and Choi, S. K. (2015). Mechanisms of Drug Release in Nanotherapeutic Delivery Systems. Chem. Rev. *115*, 3388-3432.

37. Zou, P., Chen, H., Paholak, H. J., Sun, D. (2013). Noninvasive Fluorescence Resonance Energy Transfer Imaging of *In Vivo* Premature Drug Release from Polymeric Nanoparticles. Mol. Pharmaceutics *10*, 4185-4194.

38. Lu, J., Owen, S. C., Shoichet, M. S. (2011). Stability of Self-Assembled Polymeric Micelles in Serum. Macromolecules *44*, 6002-6008.

39. Savic, R., Azzam, T., Eisenberg, A., Maysinger, D. (2006). Assessment of the Integrity of Poly(caprolactone)-*b*-poly(ethylene oxide) Micelles under Biological Conditions: A Fluorogenic-Based Approach. Langmuir *22*, 3570-3578.

40. Chen, H., Kim, S., He, W., Wang, H., Low, P. S., Park, K., Cheng, J. X. (2008). Fast Release of Lipophilic Agents from Circulating PEG-PDLLA Micelles Revealed by in Vivo Förster Resonance Energy Transfer Imaging. Langmuir *24*, 5213-5217.

41. Diezi, T. A., Bae, Y., Kwon, G. S. (2010). Enhanced Stability of PEG-block-poly(N-hexyl stearate l-aspartamide) Micelles in the Presence of Serum Proteins. Mol. Pharm. *7*, 1355-1360.

42. Zhang, X., Malhotra, S., Molina, M., and Haag, R. (2015). Micro- and Nanogels with Labile Crosslinks-from Synthesis to Biomedical Applications. Chem. Soc. Rev. *44*, 1948-1973.

43. Dai, Y., Chen, X., and Zhang, X. (2018). Recent Developments in the Area of Click-Crosslinked Nanocarriers for Drug Delivery. Macromol. Rapid Commun. 1800541.

44. Liu, B., and Thayumanavan, S. (2017). Substituent Effects on the pH Sensitivity of Acetals and Ketals and Their Correlation with Encapsulation Stability in Polymeric Nanogels. J. Am. Chem. Soc. *139*, 2306-2317.

45. Ryu, J., Chacko, R. T., Jiwpanich, S., Bickerton, S., Babu, R. P., and Thayumanavan, S. (2010). Self-Cross-Linked Polymer Nanogels: A Versatile Nanoscopic Drug Delivery Platform. J. Am. Chem. Soc. *132*, 17227-17235.

46. Kamphuis, M. M. J., Johnston, A. P. R., Such, G. K., Dam, H. H., Evans, R. A., Scott, A. M., Nice, E. C., Heath, J. K., and Caruso, F. (2010). Targeting of Cancer Cells Using Click-Functionalized Polymer Capsules. J. Am. Chem. Soc. *132*, 15881-15883.

47. Joralemon, M. J., O'Reilly, R. K., Hawker, C. J., and Wooley, K. L. (2005). Shell Click-Crosslinked (SCC) Nanoparticles: A New Methodology for Synthesis and Orthogonal Functionalization. J. Am. Chem. Soc. *127*, 16892-16899.

48. Espeel, P., Goethals, F., and Prez, F. E. D. (2011). One-Pot Multistep Reactions Based on Thiolactones: Extending the Realm of Thiol-Ene Chemistry in Polymer Synthesis. J. Am. Chem. Soc. *133*, 1678-1681.

49. Lundberg, P., Hawker, C. J., Hult, A., and Malkoch, M. (2008). Click Assisted One-Pot Multi-Step Reactions in Polymer Science: Accelerated Synthetic Protocols. Macromol. Rapid Commun. *29*, 998-1015.

50. Dömling, A., Wang, W., and Wang, K. (2012). Chemistry and Biology of Multicomponent

Reactions. Chem. Rev. *112*, 3083–3135.

51. Rotstein, B. H., Zaretsky, S., Rai, V., and Yudin, A. K. (2014). Small Heterocycles in Multicomponent Reactions. Chem. Rev. *114*, 8323-8359.

52. Touré, B. B., and Hall, D. G. (2009). Natural Product Synthesis Using Multicomponent Reaction Strategies. Chem. Rev. *109*, 4439–4486.

53. Wessjohann, L. A., Rivera, D. G., and Vercillo, O. E. (2009). Multiple Multicomponent Macrocyclizations (MiBs): A Strategic Development Toward Macrocycle Diversity. Chem. Rev. *109*, 796–814.

54. Kreye, O., Tóth, T., and Meier, M. A. R. (2011). Introducing Multicomponent Reactions to Polymer Science: Passerini Reactions of Renewable Monomers. J. Am. Chem. Soc. *133*, 1790-1792.

55. Solleder, S. C., and Meier, M. A. R. (2014). Sequence Control in Polymer Chemistry through the PasseriniThree-Component Reaction. Angew. Chem. Int. Ed. *53*, 711-714.

56. Kakuchi, R., and Theato, P. (2013). Three-Component Reactions for Post-Polymerization Modifications. ACS Macro Lett. *2*, 419-422.

57. Deng, X., Du, F., and Li, Z. (2014). Combination of Orthogonal ABB and ABC Multicomponent Reactions toward Efficient Divergent Synthesis of Dendrimers with Structural Diversity. ACS Macro Lett. *3*, 667-670.

58. Deng, X., Cui, Y., Du, F., and Li, Z. (2014). Functional Highly Branched Polymers from Multicomponent Polymerization (MCP) Based on the ABC Type Passerini Reaction. Polym. Chem. *5*, 3316-3320.

59. Yang, B., Zhao, Y., Fu, C., Zhu, C., Zhang, Y., Wang, S., Wei, Y., and Tao L. (2014). Introducing the Ugi Reaction into Polymer Chemistry as a Green Click Reaction to Prepare Middle-Functional Block Copolymers. Polym. Chem. *5*, 2704-2708.

60. Lee, I. H., Kim, H., and Choi, T. L. (2013). Cu-Catalyzed Multicomponent Polymerization to Synthesize a Library of Poly(N-sulfonylamidines). J. Am. Chem. Soc. *135*, 3760-3763.

61. Lee, M. H., Yang, Z., Lim, C. W., Lee, Y. H., Dongbang, S., Kang, C., and Kim, J. S. (2013). Disulfide-Cleavage-Triggered Chemosensors and Their Biological Applications. Chem. Rev. *113*, 5071-5109.

62. Hoshyar, N., Gray, S., Han, H., and Bao, G. (2016). The Effect of Nanoparticle Size on *in vivo* Pharmacokinetics and Cellular Interaction. Nanomedicine *11*, 673-692.

63. Badi, N., and Lutz, J. F. (2009). PEG-based Thermogels: Applicability in Physiological Media. J. Controlled Release *140*, 224-229.

64. Aathimanikandan, S. V., Savariar, E. N., and Thayumanavan, S. (2005). Temperature-Sensitive Dendritic Micelles J. Am. Chem. Soc. *127*, 14922-14929.

65. Xiao, K., Li, Y., Luo, J., Lee, J. S., Xiao, W., Gonik, A. M., Agarwal, R. G., and Lam, K. S. (2011). The Effect of Surface Charge on *in vivo* Biodistribution of PEG-Oligocholic Acid Based Micellar Nanoparticles. Biomaterials *32*, 3435-3446.

66. Sakhrani, N. M., and Padh, H. (2013). Organelle Targeting: Third Level of Drug Targeting. Drug Des. Devel. Ther. *7*, 585-599.

67. Jiwpanich, S., Ryu, J., Bickerton, S., and Thayumanavan, S. (2010). Noncovalent Encapsulation Stabilities in Supramolecular Nanoassemblies. J. Am. Chem. Soc. *132*, 10683-10685.

68. Liu, B., and Thayumanavan, S. (2017). Importance of Evaluating Dynamic Encapsulation Stability of Amphiphilic Assemblies in Serum. Biomacromolecules *18*, 4163-4170.

TOC Graphic

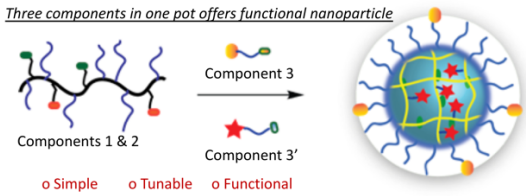
Three components in one pot offers functional nanoparticle
Components 1 & 2
Component 3
Component 3′
o Simple
o Tunable
o Functional